BIROn - Birkbeck Institutional Research Online

The relationship between kinematics and fault geometry for surface coseismic ruptures on across-strike faults: New observations of slip vectors and displacements along the Pisia and Skinos faults from the 1981 Eastern Gulf of Corinth, Greece earthquakes

Sam Mitchell [a,*], Gerald P. Roberts [a], Joanna P. Faure Walker [b], Francesco Iezzi [c], Claudia Sgambato [a], Jennifer Robertson [a], Zoë K. Mildon [d], Athanassios Ganas [e], Ioannis D. Papanikolaou [f], Elias J. Rugen [g]

[a] Department of Earth and Natural Sciences, Birkbeck College, University of London, UK
[b] Institute for Risk and Disaster Reduction, University College London, London, UK
[c] Department of Earth Sciences, Environment and Resources, University of Naples Federico II, Naples, Italy
[d] School of Geography, Earth and Environmental Sciences, University of Plymouth, UK
[e] National Observatory of Athens, Athens, Greece
[f] Agricultural University of Athens, Athens, Greece
[g] Department of Earth Sciences, University College London, London, UK

ARTICLE INFO

ABSTRACT

The relationships between kinematics and fault geometry for the coseismic ruptures from the 24th and February 25, 1981 earthquake sequence in the eastern Gulf of Corinth (Ms 6.7 and 6.4) are analysed. The two earthquakes ruptured faults located across strike rather than along strike as typifies other earthquake sequences. In detail, surface ruptures formed on the sub-parallel Pisia and Skinos Faults, with an 8 km along-strike overlap zone, separated across strike by < 2 km. The largest coseismic offsets occurred in the overlap zone. The 41-year-old ruptures are still well preserved as bedrock fault plane lichen-free stripes and colluvial ruptures, allowing detailed structural mapping at 213 rupture localities. A comparison between our measurements and Jackson et al. (1982) showed no overall consistent signal of post-seismic slip as some of our measurements were greater and some smaller than those recorded in 1981. The ruptures produced a single maximum asymmetric profile (Pisia: maximum throw of 223 cm) and a double maxima profile (Skinos: maximum throw of 109 cm and 130 cm). The shapes of the profiles differed in previous earthquakes on these faults, as evidenced by an older lichen-free stripe, implying non-characteristic earthquakes. Summing the two overlapping throw profiles across-strike reveals a single maximum symmetric bell-like profile. Using the above observations on coseismic offsets, kinematic information, and the geometry of faults, a rupture scenario has been proposed in terms of fault bends and corrugation orientations which suggests that parts of each fault may have ruptured in each earthquake.

1. Introduction

Normal faulting earthquakes have the potential to generate hazardous shaking so the need for understanding of active faulting is imperative. Surface ruptures are the expression of slip at depth and can be produced during normal faulting earthquakes, providing both direct fault displacement hazard and important insights into the manner in which faults rupture in earthquakes.

Examples of historical normal faulting earthquake sequences with detailed analysis of coseismic rupture kinematics are relatively rare. The well documented examples with surface ruptures include Sonora, Mexico (1887) (Suter, 2015), Dixie Valley and Fairview Peak, USA (1954) (Caskey et al., 1996), Irpinia, Italy (1980) (Pantosti and Valensise, 1990), Borah Peak, USA (1983) (Crone et al., 1987) and Mt Vettore, Italy (2016) (Villani et al., 2018) (Fig. 1a–e). Fault geometries and kinematic parameters along these ruptures have been measured, analysed

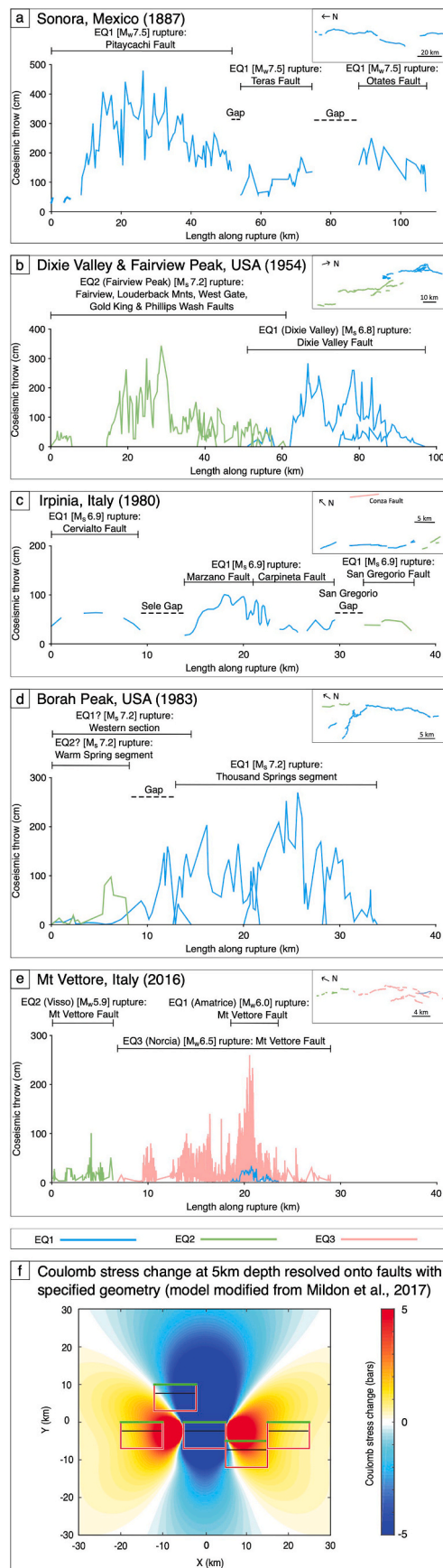**Fig. 1.** Coseismic throw profiles of ruptures along the length of faults during the following earthquake sequences: (a) Sonora, Mexico (1887) (Suter, 2015), (b) Dixie Valley and Fairview Peak, USA (1954) (Caskey et al., 1996), (c) Irpinia, Italy (1980) (Pantosti and Valensise, 1990), (d) Borah Peak, USA (1983) (Crone et al., 1987), (e) Mt Vettore, Italy (2016) (Villani et al., 2018). Blue, green, and red lines represent the faults which ruptured during each earthquake. (f) Coulomb stress transfer model showing stress transferred at a specified depth from one slipping fault onto other faults (Mildon et al., 2017). Green line is the surface trace of the faults, black line is the depth at which the Coulomb stress transfer is observed and red lines indicate the extent of the faults horizontally and vertically. (For interpretation of the references to colour in this figure legend, the reader is referred to the Web version of this article.)

and possible earthquake producing and halting mechanisms have been suggested in terms of earthquake timing, spatial fault distribution and stress transfer (e.g. Biasi and Wesnousky, 2017).

A noteworthy similarity among these earthquake sequence examples lies in the spatial arrangement of the ruptures which are, in general, positioned along-strike from each other (Fig. 1a–e). These cases involved the partial or entire rupture of individual and/or multiple faults, exhibiting displacement profiles with single to multiple maxima per fault (Suter, 2015; Caskey et al., 1996; Pantosti and Valensise, 1990; Crone et al., 1987; Villani et al., 2018). In detail, the locations of displacement maxima have commonly been observed at fault bends, where the fault steepens, resulting in an increased vertical displacement (Faure Walker et al., 2009; Mildon et al., 2016; Iezzi et al., 2018). Coulomb Stress Transfer (CST) has been proposed as a mechanism driving rupture propagation from one along-strike fault to neighbouring faults (King et al., 1994; Stein, 1999) (Fig. 1f), because stress is increased along strike.

However, our understanding of across-strike fault behaviour during individual earthquake sequences in terms of slip vectors and displacement profiles is limited. While long-term interactions between across-strike normal faults are known, e.g. the fault arrays of the rifted region of the Timor Sea, offshore north-west Australia (Meyer et al., 2002) and the faults close to Athens (Iezzi et al., 2021), with geological throws developed over thousands or millions of years, and the throw-rates averaged over shorter time periods showing patterns that reveal cooperation between faults across strike to produce the regional strain (Gupta et al., 1998; Gupta and Scholz, 2000; McLeod et al., 2000; Meyer et al., 2002; Cowie et al., 2005; Faure Walker et al., 2010; Iezzi et al., 2019), it remains unclear how or whether such interactions occur during individual earthquake sequences.

In this paper, we document the surface ruptures of two sub-parallel normal faults in the Gulf of Corinth, Greece (Fig. 2b). These faults, spaced < 2 km apart across strike where they overlap, ruptured in two Ms > 6 earthquakes within a few hours of each other in 1981. Despite the considerable time elapsed of 41 years since the earthquakes, the surface ruptures have remained exceptionally well-preserved, especially in thick forest vegetation on the north facing limestone bedrock fault scarps. Through detailed field mapping, we generate a high-resolution trace map of both faults, and collected a dense structural data set of kinematic measurements of the ruptures, with locality spacing between 10 and 100 m. Through comparison with data collected following the 1981 earthquake by Jackson et al. (1982), our data allows us to document the lack of resolvable post-seismic slip since 1981 which has previously been identified for the ruptures of the 2016 earthquakes on the Mt Vettore Fault (Iezzi et al., 2018). We have also measured changes in slip between the 1981 earthquakes and older surface rupturing earthquakes at the same locations along each fault. This example, involving the co-rupture of faults across-strike rather than along-strike, presents a rare opportunity to study this style of rupture geometry. The mapping, new measurements, and analysis of the dataset, in particular the slip vectors and the displacement profiles, offers valuable insights into rupturing scenarios, the faulting process and hazard associated with across-strike faults rupturing during an earthquake sequence.
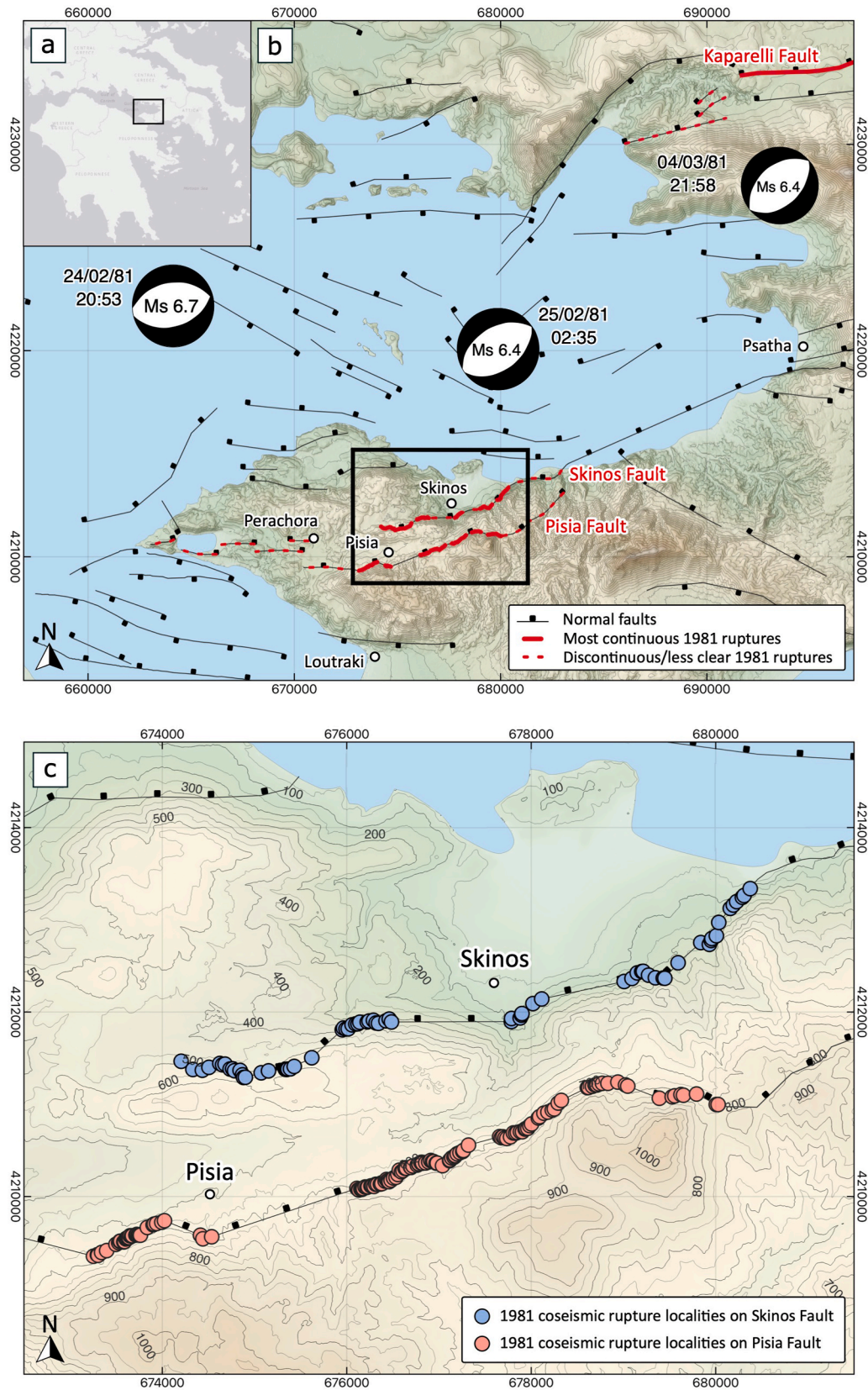
Fig. 2. Location of the 1981 coseismic ruptures on the Pisia and Skinos Faults. (a) Coastline map of mainland Greece showing location of area (b) in the black box. (b) Map of Perachora Peninsula and the eastern Gulf of Corinth region with surface traces of faults (solid) (Ganas et al., 2013) showing the location of the study area (c) in the black box. Focal mechanisms are displayed at the inferred epicentres of the three earthquakes of the 1981 eastern Gulf of Corinth earthquake sequence (Hubert et al., 1996). (c) Map of the Pisia and Skinos Faults with site locations of the 1981 surface ruptures recorded during the investigation. Coordinate system: WGS 84/UTM Zone 34 S.

2. Geological background

Extension has been ongoing across Greece for the past 5 Ma in an approximately north-south orientation producing normal faults which have overprinted previously thickened crust of the Cretaceous-Miocene Alpine fold-and-thrust belt (Billiris et al., 1991; Jackson, 1994; Clarke et al., 1998; Roberts and Ganas, 2000; Goldsworthy et al., 2002; Vassilakis et al., 2011). The extension occurs in the framework of two major tectonic processes. (1) Slab roll-back of the Hellenic subduction zone between the African and Eurasian Plates, generating back-arc extension in the overlying Eurasian plate (Jolivet et al., 1994; Jolivet, 2001). (2) Dextral motion of the North Anatolian Strike-slip Fault (Kelletat et al., 1976; Le Pichon and Angelier, 1979; Westaway, 1991; Jackson, 1994; Jolivet et al., 1994, 2013; Le Pichon et al., 1995). In central mainland Greece, the normal faults strike approximately east-west and the records of seismicity in the array of normal faults on the mainland date as far back as at least 464 BC, at which time a devastating earthquake was reported in the Sparta region by the ancient Greek philosopher Plutarch (Guidoboni et al., 1994). More recently, historical records have shown frequent, moderate-to-large destructive earthquakes (Ambraseys and Jackson, 1990) and in some instances where surface rupturing also occurred, rupture kinematics and fault geometries have been possible to record, such as the 1894 Atalanti earthquake (Ganas et al., 1998; Pantosti et al., 2001).

During the 1981 eastern Gulf of Corinth earthquake sequence, slip on the Pisia, Skinos and Kaparelli Faults caused surface rupture during three earthquakes on the 24th, 25th February and 4th March with Ms = 6.7, 6.4 and 6.4, respectively, killing 22 people (Jackson et al., 1982) (Fig. 2b). Although the arrangement of the Kaparelli Fault from the Pisia and Skinos Faults is along-strike, we focus on the across-strike ruptures of the Pisia and Skinos Faults. Interviews with the local population following the initial two earthquakes revealed that the sequence of the ruptures on the Pisia and Skinos Faults and which ruptures were associated with which of the earthquakes are unknown due to both earthquakes taking place within hours of each other overnight at 20:53 and 02:35 local time (U.S.G.S.). Structural measurements of the ruptures on both the Pisia and Skinos Faults were recorded soon after the earthquakes, at 17 localities (Jackson et al., 1982) and multiple further studies have been undertaken on both faults. However, the mapping conducted in 1981 (Jackson et al., 1982), although revolutionary in helping us understand normal faulting earthquakes in Greece and worldwide, presents lower spatial resolution and hence less detail than the data sets for the earthquake sequences shown in Fig. 1 for Mexico, the western USA and Italy (Crone et al., 1987; Pantosti and Valensise, 1990; Caskey et al., 1996; Suter, 2015; Villani et al., 2018). Furthermore, in some of these cases, revisiting the ruptures to perform additional detailed analyses has helped improve the understanding of the sequence of the rupturing events (e.g. Bello et al., 2021a; Bello et al., 2021b; Bello et al., 2022; Brozzetti et al., 2019).

The Pisia and Skinos Faults are located east of the Gulf of Corinth and north of Corinth town, near to the villages of Pisia and Skinos (Fig. 2). The Gulf of Corinth has been formed by rifting and is extending north-south with GPS-derived rates in the gulf's eastern region of 5.4 ± 1.2 mm/yr, which is lower in contrast to the gulf's western region of 10.4 mm/yr (Briole et al., 2021). The footwalls of the normal faults comprise Mesozoic limestones, as well as Neogene sediments in some places, with rare outcrops of mafic ophiolitic rocks and deep-sea cherts (Roberts and Jackson, 1991; Walker et al., 2010; Ford et al., 2013; Whittaker and Walker, 2015). Erosion of footwall rocks result in the transportation and deposition of Neogene-Holocene sediments in the hangingwall e.g. alluvium, colluvium and marine deposits (Roberts and Jackson, 1991; Goldsworthy and Jackson, 2000; Rohais et al., 2007; Taylor et al., 2011; Ford et al., 2013; Gawthorpe et al., 2018, 2022). At the surface, the north-dipping Pisia and Skinos Faults produce two half grabens. At depth, the geometry and arrangement of the faults are unknown, however, it has been speculated that the two faults link (Roberts, 1996). The

Pisia Fault is exposed at the surface for approximately 25 km with visible offsets produced by the 1981 ruptures (Roberts and Ganas, 2000). Fault measurements recorded close to the centre of the Pisia Fault, which are representative of the regional extension direction (Roberts and Ganas, 2000), indicated a north-north-west - south-south-east extension, with the average slip vector azimuth of the fault plane ranging between 350° and 358° (Mechernich et al., 2018). No evidence of earthquakes on the two faults have been identified in historical records prior to the 1981 earthquakes, however, paleoseismological analysis has revealed multiple earthquakes on both faults during the Holocene (Collier et al., 1998; Mechernich et al., 2018). Cosmogenic exposure analysis of a carbonate fault scarp on the Pisia Fault has been interpreted to show six to eight moderate-large paleoearthquakes during the Holocene, with an average slip-rate of 0.5–0.6 mm/yr (Mechernich et al., 2018). Radiocarbon trench analysis of the Bambakies fan on the Skinos Fault revealed an average throw-rate of 0.7–2.5 mm/yr with up to six previous paleoearthquakes which were comparable to the displacements produced during the 1981 earthquakes (Collier et al., 1998).

3. Methods

Detailed structural mapping was undertaken during April and June 2022 along the 1981 ruptures on the Pisia and Skinos Faults, 41 years after the earthquakes. Ruptures were recorded at 146 and 67 localities on the Pisia and Skinos Faults, respectively, using a handheld Garmin GPS, with a location accuracy of ±5 m (Fig. 2c).

The ruptures were identified in the form of several tectono-geomorphic features; lichen-free stripes on limestone bedrock fault scarps; colluvial ruptures (soil steps); and a ground crack (Fig. 3). Structural measurements of the ruptures were recorded including strike, dip, slip vector azimuth, slip vector plunge, coseismic throw, coseismic heave and coseismic slip, and were collected using a compass clinometer and measuring tape (Fig. 3a).

The tops of lichen-free stripes (Fig. 3 S1-10,P2-3,P5-12) define lines suspected to be where the hangingwall ground surface met the fault plane prior to the 1981 earthquakes as the base of the lichen is parallel to the ground surface; above this line, greyish white lichen can be identified on bedrock fault plane and below this line, grey lichen-free bedrock fault plane can be observed. The top of the lichen-free stripe may, in places, also have soil, plants or trees which appear to be snapped or broken away from the ground surface. The stripes can only be measured at sites which exclude gullies and fans, whereby the stripe line is parallel to the hangingwall cut-off. This is based on the assumption that all exhumation, or at least the entire thickness of the lichen-free zone, is due to tectonic causes without the influence of other factors, such as gravity or compaction of deposits at the hangingwall (e.g. Bello et al., 2022b, their Fig. 5). The vertical extent of the lichen-free stripes, alongside kinematic measurements of slip direction from corrugations and frictional wear striae, can be used to determine the slip, heave, and throw, of the ruptures. The strike and dip of the fault can be measured on the bedrock fault plane.

Soil steps (Fig. 3P1,P5) are breaks in slope where soil has been offset, with exposed hangingwall colluvium, broken roots, and fallen trees in places. The general strike can be measured along the length of the offset soil and throw can be measured using geomorphic piercing points, which are parts of objects that have separated during rupturing allowing the amount of displacement to be determined such as places where rock clasts or parts of trees could be seen to have fitted into cavities on the opposite side of the rupture.

Ground cracks primarily form in association with a few to 10 s cm wide openings. The strike can be measured along the length of the crack and kinematic measurements can be measured using geomorphic piercing points.

The measurement uncertainties including those due to human error and eroded and uneven fault surfaces are presented in Table 1. Measurements were recorded in numerous locations at every observable

Fig. 3. Tectono-geomorphological evidence of the 1981 coseismic ruptures on the Pisia and Skinos Faults. (a) (i) Rupture on a carbonate normal fault scarp displayed in the form of a lichen-free stripe. (ii) Structural measurement data collection method using a tape measure. (b) Map of localities of the rupture evidence in (c) on the Skinos (blue) and Pisia (red) Faults. (c) Photographs of 1981 ruptures. (S1–S10) Skinos Fault ruptures in the form of lichen stripes. (P1–P12) Pisia Fault ruptures. black arrows/white borders = lichen stripe location. White arrows/black borders = vertical displacement direction of hangingwall on a soil step. (For interpretation of the references to colour in this figure legend, the reader is referred to the Web version of this article.)

Table 1
Structural measurement uncertainties per tectono-geomorphic feature. - = unable to collect measurement on the geologic feature.

	Bedrock fault scarp	Soil step	Ground crack
Strike (°)	±2.5	±5.0	±20
Dip (°)	±1.5	–	–
Plunge (°)	±1.5	–	±1.5
Plunge Direction (°)	±2.5	–	±2.5
Coseismic slip (cm)	±1.5	–	±1.5
Coseismic heave (cm)	±1.5	–	±1.5
Coseismic throw (cm)	±1.5	±5.0	±1.5

rupture and where on individual long exposures of the ruptures greater than 10 m, measurements were taken every ~10 m along strike. The structural measurements were plotted along a line oriented parallel to eastings 673,000-681000 m of coordinate system WGS 84/UTM Zone 34 S (Fig. 4). In addition, the measurements were plotted on stereonets using the software "Stereonet 10.0" (Allmendinger et al., 2011), as shown in Fig. 5b.

The collected structural data were compiled, and the following analyses were conducted. (1) Identification and comparisons of our structural measurement patterns along the strike of the faults and between the two faults to constrain how the rupture style relates to fault geometry. (2) Examination of our structural measurements with stereonets to identify patterns in slip vector azimuths along the strike of both faults. (3) Comparison of our data to previous measurements (Jackson et al., 1982) on the faults to assess post-seismic slip. (4) Comparison, using our data and one site of Mechernich et al. (2018), of the coseismic throws of the 1981 ruptures to prior ruptures on both faults to assess possible changes in rupture styles. (5) Summation of the coseismic throws of the two across-strike faults to produce a composite summed coseismic throw profile by a discretisation approach. The throw profiles are the vertical displacements along the strike of the ruptured faults and are derived from mostly our data with some measurements in the eastern regions of the Skinos Fault from Collier et al. (1998).

In order to interpret the slip vectors (Fig. 5), measurements were split into eight areas; four areas for the Skinos Fault (Area S1–S4) and four areas for the Pisia Fault (Area P1–P4), across strike from each other. Stereonets were used to analyse all data in each area (Fig. 5b). Strike and dip measurements were used to obtain a pole to the b-axis. Mean values of the plunge and plunge direction were calculated with 99% confidence intervals of each area. Both the poles to b-axis and mean slip vectors are displayed together on the stereonets as both forms of measurement show the direction in which the fault slips and should be similar (Roberts, 2007).

The comparison of our throw data to previously published throw measurements required the conversion of Jackson et al. (1982)'s measurements of dip and amplitude of slip to throw values (Fig. 6a).

An along-strike throw profile which combines the Pisia and Skinos throws was achieved by discretising both sets of coseismic throws and summing the discretised throws across-strike (Fig. 7). The throw profiles for each fault were discretised because measurements were not collected at the same easting on both faults, therefore, discretisation was undertaken by sampling throw values from the throw profiles every 200 m easting over the study area of 10 km between the eastings of 673,000 and 683,000 m. A summed coseismic throw distribution was then produced by summing the sampled throw values from both faults together.

4. Results

4.1. Field observations of ruptures

Evidence of the 1981 ruptures were identified in many places on both the Pisia and Skinos Faults (Figs. 3–6). The most commonly identified evidence of the ruptures were the lichen-free stripes on limestone bedrock fault scarps (Fig. 3a,3cS1-10,P2–P4,P6–P12). In some eastern parts of the studied area of the Skinos Fault, the lichen-free stripes appeared as scorched surfaces, these were interpreted as where lichen were previously present and were burned due to the 2021 wildfires (Fig.3cS8,9,10). Soil steps were identified in places along the western parts of studied area of the Pisia Fault (Fig. 3cP1,P5), however, it was generally not possible or very challenging to identify geomorphic piercing points and therefore to measure slip vectors, although some examples were noted. One ground crack was identified with a possible geomorphic piercing point, although it was challenging to interpret, in cemented beach deposits on the south side of Lake Vouliagmeni. It is fortuitous that we were able to record the piercing points given the fragility of such features, and perhaps the north-facing slope with thick stabilising vegetation has helped.

4.2. Analysis of structural measurements

Kinematic measurements were concentrated along the most continuously preserved portion of the 1981 ruptures at 146 and 67 localities along the Pisia and Skinos Faults, respectively (Fig. 2c). Analysis of the kinematics revealed various trends on both faults and similarities and differences between the faults.

In this study area with concentrated measurements, both the Pisia and Skinos Faults have an overall strike of west-south-west, while the strikes of the fault planes at any local site measured between 176 and 341° for the Skinos Fault and 190 to 340° for the Pisia Fault (Fig. 4ai,bi). Along both faults, the strike varied by up to ±45° every few to tens of meters along the strike of the faults. The average values of the strikes of the faults (modes) differ slightly; the mode of the strike for the Skinos Fault was between west to west-north-west and the mode of the strike for the Pisia Fault was between west-south-west to west (see histograms on Fig. 4a and b). The general pattern of the range of strikes along the length of the faults differ; from west to east the strike of the fault planes measured generally change from west-north-west to south-west. In contrast, the Pisia Fault showed strikes ranging between south to west-north-west for 6 km between the eastings of 673,000–679,000 m, however, at the easternmost 2 km of the ruptures, from 679,000 to 6,810,000 m, the general range of strikes changes to approximately north-west (Fig. 4ai,bi).

The dips on both faults showed changes every few metres to tens of meters along the strike of the faults. For the Skinos Fault, dip values ranged from 50° to 88°, while the Pisia Fault displayed a larger dip variability, ranging between 36° and 88° (Fig. 4aii,bii). The dip of the Pisia Fault is steeper than the Skinos Fault dip by 5° to 10°, based on the mode values; the Pisia Fault has a mode dip of 60° to 70° and the Skinos Fault has a mode dip of 55° to 65° (see histograms in Fig. 4aii and 4bii). A notable localised cluster of steeper dips, 80° to 90°, on the Pisia Fault was identified near the 679,000 m easting. We note a small number of very low angle (e.g. 36°) fault planes in our data. We think that these are perhaps unlikely to be representative of the dip at depth, but we report them for completeness.

The plunges of slip vectors ranged between 46° to 80° for the Skinos
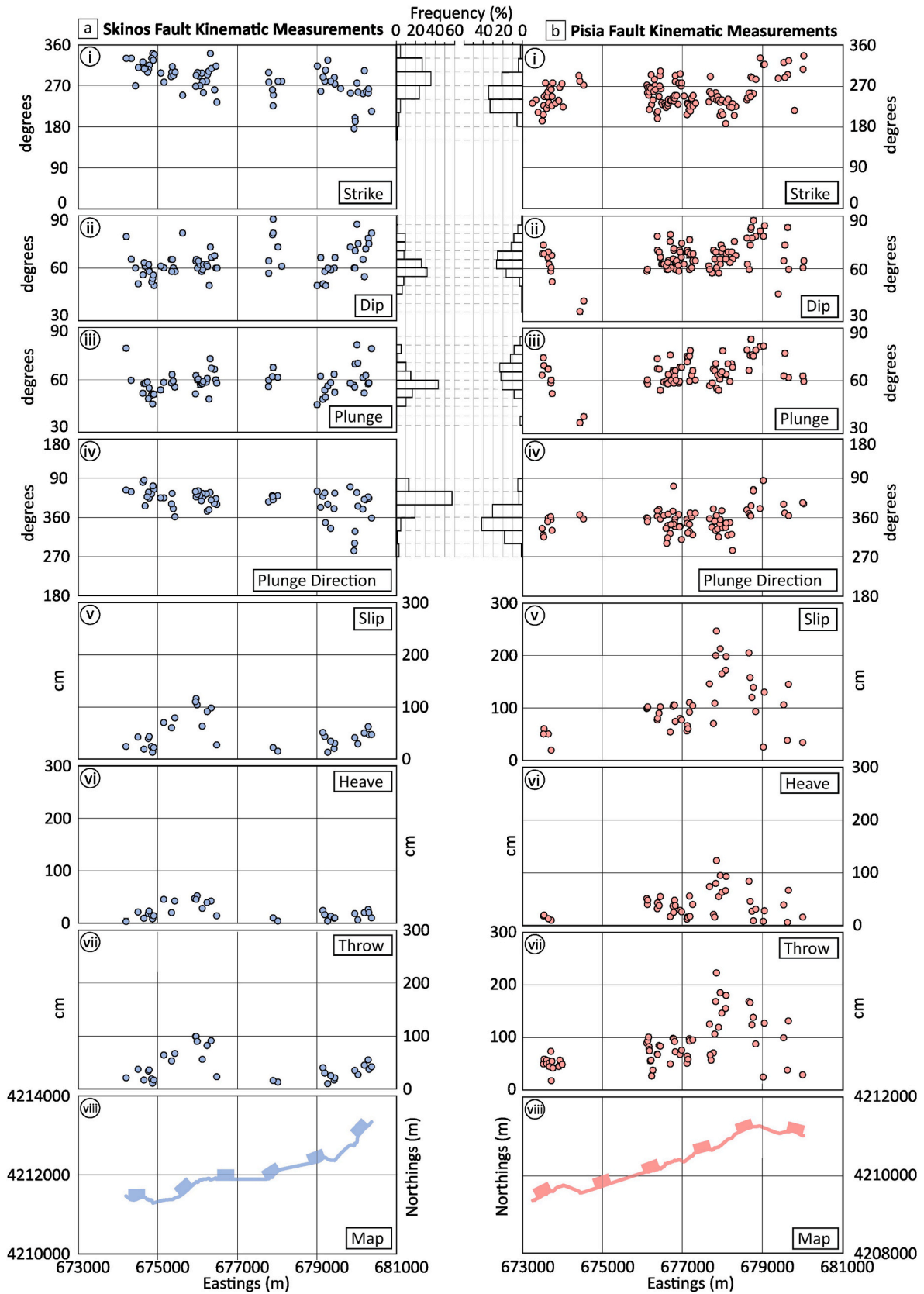
Fig. 4. Field structural data of the 1981 coseismic ruptures on the (a) Skinos and (b) Pisia Faults. Error bars presented in the table of the methods section are too small so are not visible on all graphs but are visible on ii, iii and iv. Histograms are displayed as a frequency percentage per measurement.
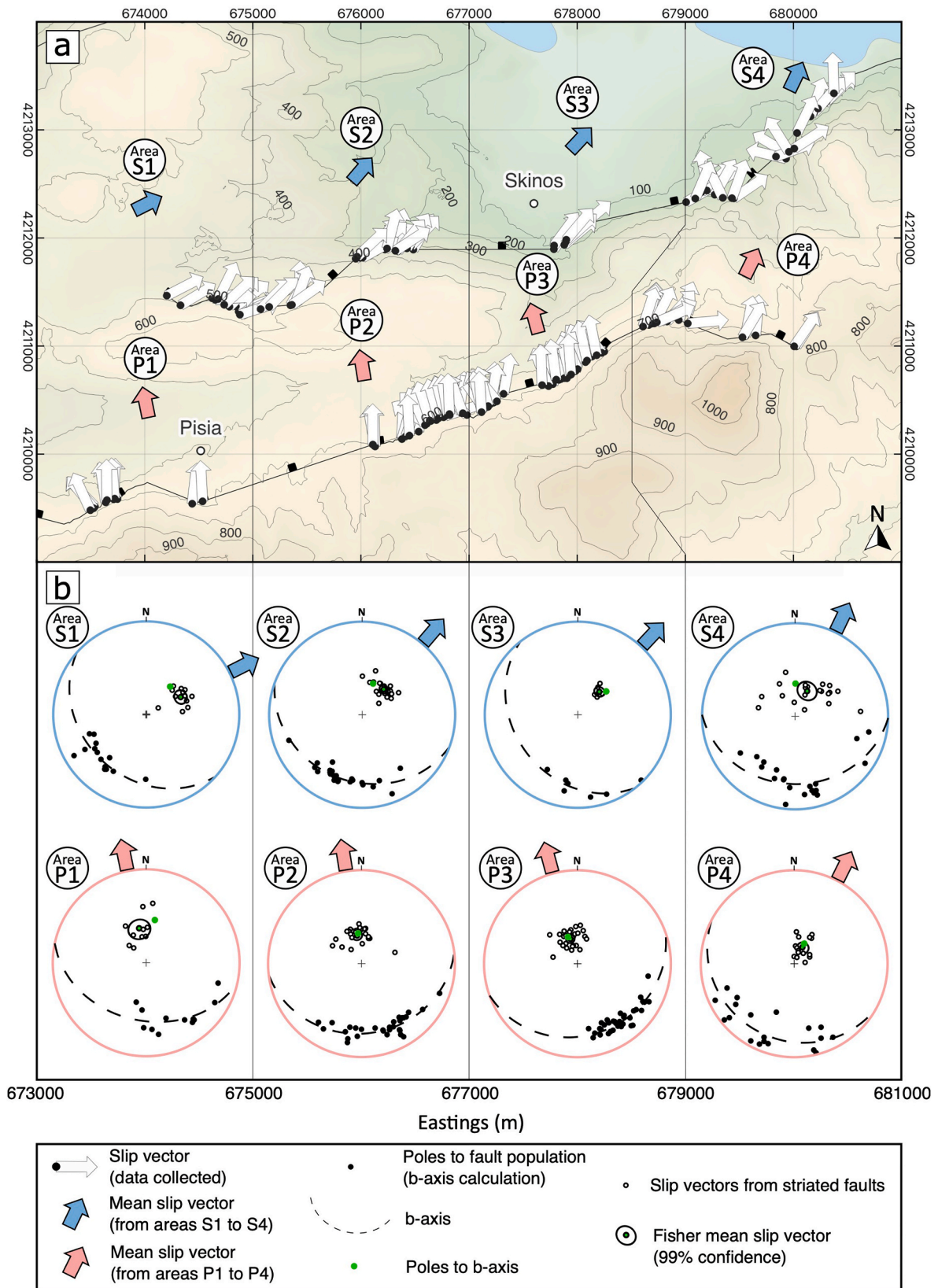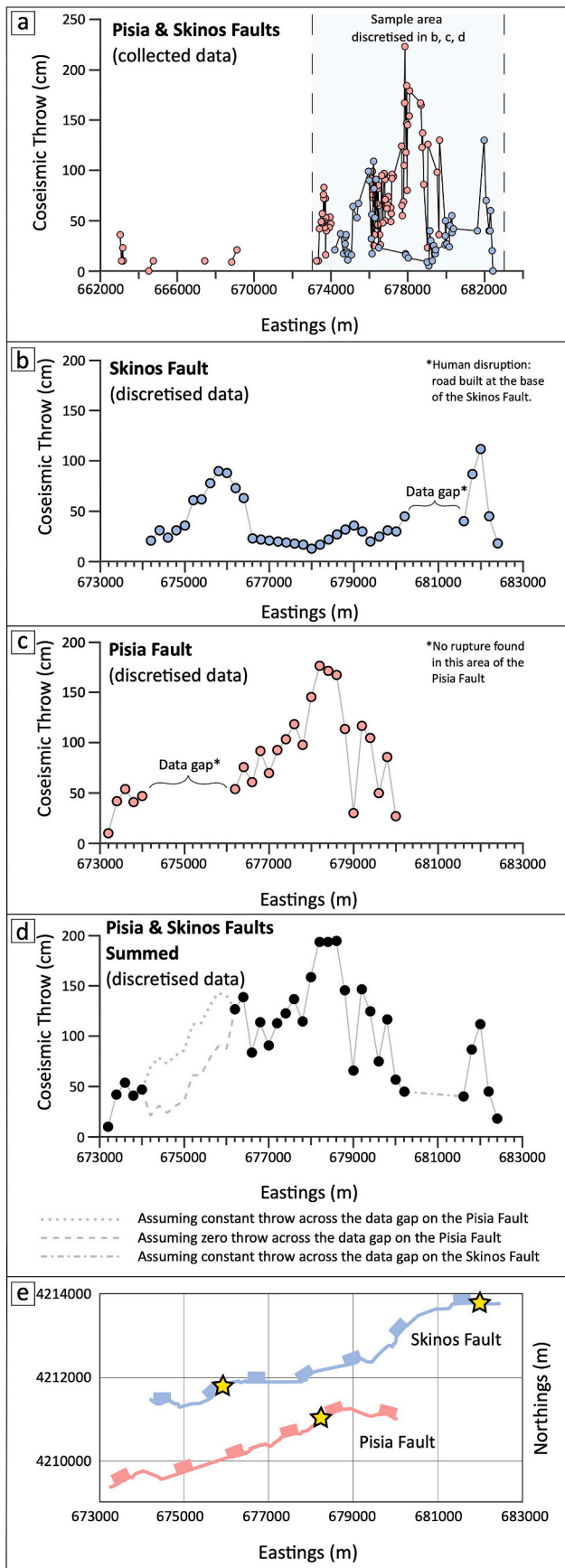
Fig. 5. Slip directions on the Pisia and Skinos Faults. (a) Map of Pisia and Skinos Faults. black dot/white arrow = individual slip direction taken at one locality, blue arrows/Area S1–S4 = Skinos Fault average slip direction across a 2 km easting, red arrows/Area P1–P4 = Pisia Fault average slip direction across a 2 km easting, except P3 data is averaged across a 1.5 km easting and P4 across a 2.5 km easting. (b) Stereonets for each area (S1–P4) comprising plunge/plunge direction and strike/dip data. (For interpretation of the references to colour in this figure legend, the reader is referred to the Web version of this article.)
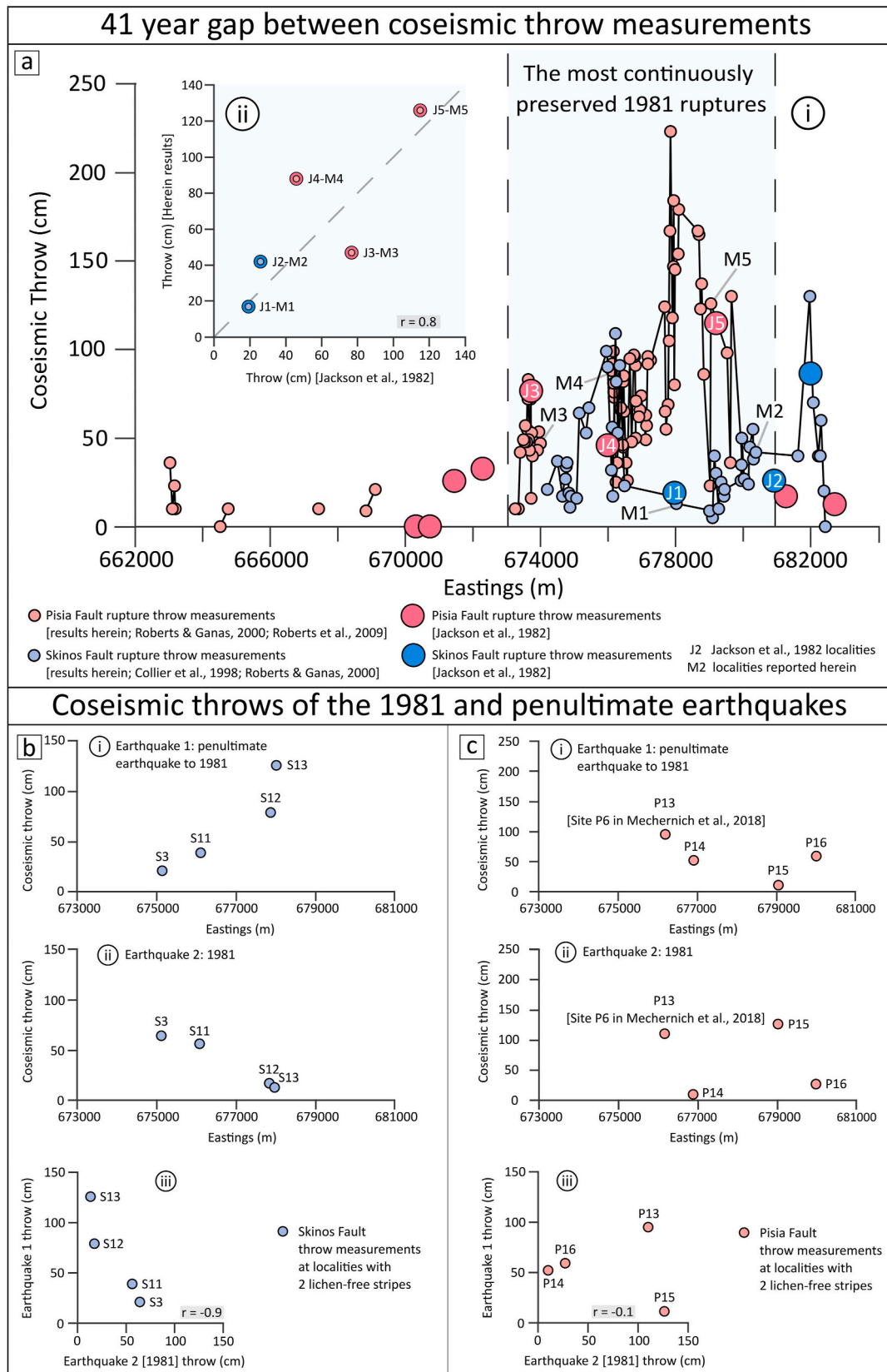
Fig. 6. Comparing coseismic ruptures on the Pisia and Skinos Faults. (a) Comparing coseismic throw measurements over 41 years since the 1981 earthquakes. (i) Coseismic throw profile of the Pisia and Skinos Fault ruptures using results recorded herein, Jackson et al. (1982), Collier et al. (1998), Roberts and Ganas (2000) and Roberts et al. (2009). (ii) Comparing our data, collected 41 years after the 1981 earthquakes, to data collected in proximal locations soon after the 1981 earthquakes (Jackson et al., 1982). Coseismic throw measurements on the (b) Skinos and (c) Pisia Faults where two lichen stripes were recorded. (i) Coseismic throw measurements of the top lichen stripe/the penultimate rupture to 1981. (ii) Coseismic throw data of the bottom lichen stripe/the 1981 rupture. (iii) Comparing coseismic throw data of the 1981 and penultimate ruptures.

Fault, while the Pisia Fault displayed a larger plunge variability, ranging between 37° to 84° (Fig. 4aiii, bii). The plunge value of the Pisia Fault is steeper than the Skinos Fault by 5° to 10°, based on the mode values; the Pisia Fault has a mode plunge of 65° to 70° and the Skinos Fault has a mode plunge of 55° to 60° (see histograms on Fig. 4aii and 4bii). The changes in plunge angles reflect the changes in fault dip.

The trends of slip vectors reveals that the Pisia and Skinos Faults have different values from west to east along both faults with the major changes occurring on both faults at 679,000 m (Fig. 4aiv,biv). The values for plunge direction vary from between north and west in the western 6 km of the Skinos Fault to between north and west in the eastern 2 km of the Skinos Fault. The trends of slip vectors for the Pisia Fault vary between west-north-west and north-north-east in the western 6 km to north and east-south-east in the eastern 2 km. Both faults show variations in plunge direction by ± 45° every few meters to tens of meters along the strike of the faults, and this is analysed further below (see Fig. 5 for further plunge direction analysis using stereonets).

The coseismic slip, heave and throw reveal numerous spatial variations along both faults, however, the loci of maximum surface displacements are different between faults (Fig. 4av,vi,vii,bv,vi,vii). In general, the Skinos Fault reveals a double-humped asymmetric spatial throw distribution with, for example, maximum throws of 109 cm at the easting of 676,222 m and 130 cm at 681,971 m, with the latter measurement obtained from Cowie and Shipton, 1998) (see Fig. 4avii for measurements obtained in this study and see Fig. 7a for the full extent of measurements). The Pisia Fault reveals a single-humped asymmetric bell-like spatial throw distribution, with the greatest values of throw of 223 m at the easting of 677,849 m (Fig. 4bvii).

4.3. Slip vector stereonet analysis

The stereonet analysis of the kinematic measurements of Area S1 to Area S4 and Area P1 to Area P4 revealed mostly convergence of slip vectors along the length of both faults whereby the slip vectors point towards the centre of the ruptured section of the fault (Fig. 5). However, some divergence of slip vectors was observed on the Pisia Fault, whereby the slip vectors point away from the centre of the ruptured fault. Along the Skinos Fault, from Area S1 to Area S4, the Fisher mean averages of the slip vectors revealed spatial variation and convergence; east-north-east, 063°, in Area S1 to north-north-east, 026°, in Area S4. Along the Pisia Fault, from Area P1 to Area P3, the Fisher mean slip vectors are between north and north-north-west and slightly converge from Area P1 to Area P3 with azimuths of 349° and 345°, respectively. However, the slip vector of P4 clearly diverges from the slip vectors of Area P3 and the Fisher mean slip vector points north-north-east with an azimuth of 028° at Area P4. The divergence of the average slip vectors from Area P3 to Area P4 occurs around the easting of 679,000 m.

4.4. Coseismic throw comparisons with previous studies

Coseismic throw comparisons between our measurements and measurements collected soon after the earthquakes in 1981 (Jackson et al., 1982) on the Pisia and Skinos Faults revealed minimal differences in throw, as quantified below (Fig. 6a). Five throw measurements taken

on the ruptures of the Pisia and Skinos Faults soon after the earthquakes were compared with our five closest measurements (Fig. 6aii). Three of our measurements, at M2, M4 and M5, were larger than the measurements at the closest localities recorded 41 years prior, at J2, J4 and J5, by 16, 42 and 11 cm, respectively. However, the other two throw measurements we recorded, at M1 and M3, were smaller than those at the closest localities recorded 41 years prior, at J1 and J3, by 2 and 29 cm, respectively. In addition, the Pearson correlation coefficient of the ten measurements described herein is 0.8, implying a strong positive correlation. Overall, the throw measurements show no resolvable difference across the 41-year gap between the data collections indicating no evidence for systematic throw changes since 1982, during the post-seismic period. It is worth noting that the comparisons may be imprecise because no hand-held GPS readings of the localities could be taken at the time when Jackson et al. (1982) undertook their field work. Despite this, the coseismic throws of the entire ruptures show that the Jackson et al. (1982) and our results are comparable (Fig. 6a).

4.5. Coseismic throw comparisons with previous events

Evidence for previous earthquakes on the Pisia and Skinos Faults, prior to the 1981 earthquakes, can be observed on the same bedrock fault scarp by identifying double lichen-free stripes, such as sites S3 and P3 (Fig. 3). It is unclear how these relate to the 6 paleoseismic earthquakes suggested by Collier et al. (1998) from paleoseismic trenching on the Skinos Fault. Double lichen-free stripes were rarely observed, however, a number of localities included double lichen-free stripes; four localities on the Skinos Fault and four on the Pisia Fault (Fig. 6bi,ii,ci,ii). Comparisons between Fig. 6bi and 6bii, along the Skinos Fault, show that our measurements of throw in the penultimate slip event were smaller than the throw values of 1981 slip event at sites S3 and S11 by 43 and 17 cm, respectively. However, throw values were greater in the penultimate slip event than in the 1981 slip event at sites S12 and S13 by 62 and 113 cm, respectively. Comparisons between Fig. 6ci and 6cii, along the Pisia Fault, show that our and Mechernich et al. (2018)'s measurements of throw in the penultimate slip event were smaller than the throw values of 1981 slip event at sites P13 (site P6 in Mechernich et al., 2018) and P15 by 15 and 115 cm, respectively. Yet, throw values were greater in the penultimate slip event than in the 1981 slip event at sites at P14 and P16 by 42 and 32 cm, respectively. In addition, comparisons of the penultimate and 1981 rupture throw measurements for the Pisia and Skinos Faults (see Fig. 6bii and 6cii) show that the spatial throw distributions changed from one earthquake to the next, suggesting that slip at the surface on each fault is non-characteristic (see Roberts (1996) for a similar conclusion and Mechernich et al. (2018) in which an irregular slip-per-event history was suggested at one locality on the Pisia Fault).

4.6. Summing the coseismic throw profiles across the two faults

Summing the discretised Pisia Fault and Skinos Fault coseismic throws produced a composite summed coseismic throw profile (similar to slip distribution but herein we measure the vertical component of slip) which generally displayed a single-humped symmetric bell-like curve (Fig. 7). To gain this combined throw profile of the across-strike ruptures, we discretised the throw profiles of the most continuous ruptures on the Pisia and Skinos Faults by taking a sample measurement from throw lines every 200 m easting along 10 km of the ruptures between the eastings of 673,000 m and 683,000 m. The ruptures on the Skinos Fault revealed a generally symmetrical throw profile comprising two peaks in throw at 675,800 m and 682,000 m; the two peaks were located towards the extremities of the zone of overlap (Fig. 7b). The ruptures on the Pisia Fault displayed an asymmetrical throw profile with one peak at 678,000 m; this single peak lies between the two peaks on the Skinos Fault (Fig. 7c). However, by summing the two discretised throw profiles across strike, the combined throw profile generally

revealed a symmetrical profile with one prominent peak in the centre around 678,000 m (Fig. 7d). The profile could also be described as a symmetrical three peaked throw profile. We note that there are data gaps on both faults and have attributed these to the ruptures being possibly eroded away or removed due to human influence (Fig. 7b and c). So, multiple assumed throw profile scenarios are displayed in those regions to show that the faults could possibly had either no coseismic throw or constant coseismic throw (Fig. 7d).

5. Discussion

The ruptures to the 1981 earthquake sequence occurred across strike from each other with displacements that when summed produce a single symmetrical throw profile in the zone of overlap between the Pisia and Skinos Faults (Fig. 7), implying interaction. This pattern differs from the overall pattern of the ruptures from other well-documented normal earthquake sequences from around the world where successive ruptures occurred predominantly along strike (Fig. 1). This has important implications for our understanding of normal faulting earthquake sequences.

The generally accepted view after an earthquake is that the hazard will have moved along strike because (a) that is where successive earthquakes have occurred in the well-documented earthquake sequences (Suter, 2015; Caskey et al., 1996; Pantosti and Valensise, 1990; Crone et al., 1987; Villani et al., 2018) highlighted in Fig. 1a–e, as well as in the 1981 earthquakes from the Pisia and Skinos Faults to the Kaparelli Fault (Jackson et al., 1982) and (b) calculations of stress change show that stress that drives ruptures is increased along strike (King et al., 1994; Stein, 1999) (Fig. 1f). The data in this paper show that in some circumstances a fault located across strike can rupture. In particular, in the Pisia-Skinos example, successive ruptures occur in the zone of overlap between two faults. The reasons this occurred are unclear, as are the exact rupture sequence through time because the two earthquakes occurred overnight, and we cannot know which part of the fault system was ruptured by each earthquake. What is clear is that rupture of the Pisia Fault or the Skinos Fault alone was not enough to release the stored elastic strain that had accumulated prior to the 1981 sequence; it appears that the faults interacted to release this stored stress.

In detail, at the surface, the Pisia and Skinos Faults are not connected due to their parallel arrangement, however, they are closely spaced (separated by < 1–2 km) and it is unknown whether the two faults are connected at depth. Therefore, the interactions between the faults at depth during the 1981 earthquakes are uncertain, and could be a number of possibilities, such as, (a) simultaneous slip of both faults with linkage at depth, (b) static stress transmitted through rigid crust from the first earthquake if there is no linkage at depth, or (c) differential stress changes within a shared shear zone in ductile crust after the first earthquake if the two faults are linked at depth. The following slip event scenarios could have taken place based on these interaction possibilities: i) based on (a), both faults ruptured together during eastward propagation of the 24/2/81 event (event 1), with the 25/2/81 event (event 2) rupturing further east and offshore, ii) also based on (a), both faults ruptured in event 2 only (see Abercrombie et al., 1995, their Fig. 10), iii) based on (b) or (c), the Pisia Fault ruptured in event 1 and Skinos Fault in event 2 (or vice versa), and/or, iv) also based on (b) or (c), parts of each fault ruptured in both events. Overall, it is challenging to determine which scenario is correct due to not knowing the linkages of the two faults at depth and the interactions between them, however, our results imply that scenario (iv) may have occurred because of the change in kinematics on the Pisia Fault (Fig. 5). Below we discuss how our findings suggest interactions between the two faults.

In the Pisia-Skinos example, slip maxima that appear as peaks on the throw profiles seem to fill in gaps of slip across strike (Figs. 6 and 7). This implies that, at least in the zone of overlap, across strike faults interact in that slip from one plus slip from the other combine to make the final

finite strain from the whole earthquake sequence considered herein, so not all the stored elastic strain that accumulated prior to 1981 was released when the first earthquake occurred. This is not an unprecedented finding. For example, the 2004 earthquake on the Parkfield segment of the San Andreas Fault filled a slip deficit that remained after the 1966 earthquake and intervening interseismic motion (Bakun et al., 2005). However, although not unprecedented, for the 1981 sequence, it

is implied that a mechanism exists that produces this temporal and spatial interaction, but the nature of this mechanism remains unclear. It could be that there is something unusual about the fault geometry for Pisia-Skinos compared to the other examples in Fig. 1. For example, the Pisia and Skinos Faults are very close together, separated by < 1–2 km across strike, and may indeed link at depth, but none the less bends in the fault traces have an amplitude in map view of ~0.5–1.5 km, so
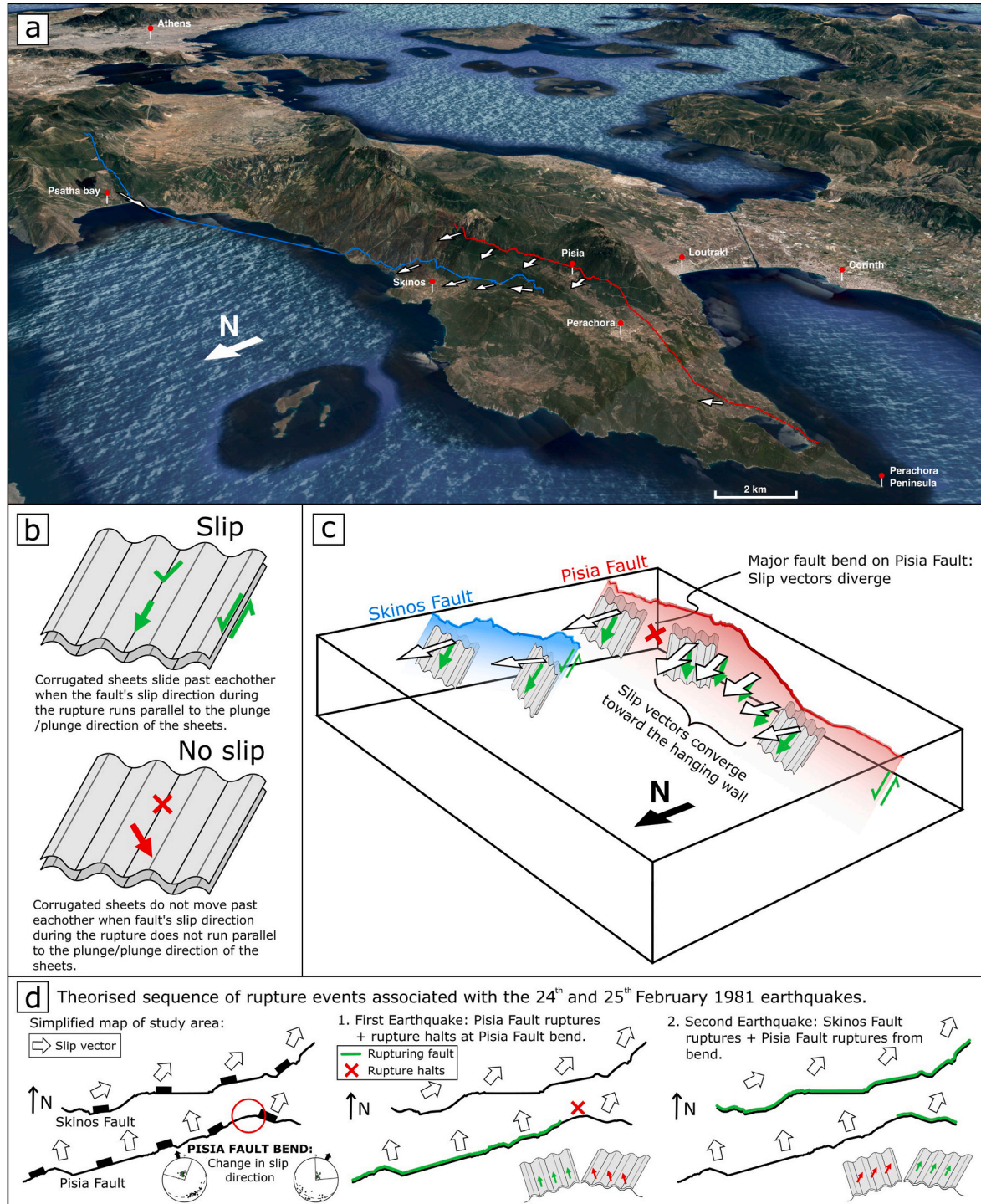
Fig. 8. A possible mechanism for the ruptures on the Pisia and Skinos Faults during the 1981 eastern Gulf of Corinth earthquake sequence. (a) 3D tectonic map of the Perachora peninsula showing the Pisia (red) and Skinos (blue) Fault traces and the averaged slip directions from this study and Roberts and Ganas (2000) at Perachora and Psatha bay (white arrows). (b) Corrugated sheets used to explain slip on faults between two blocks. (c) Simple 3D interpretation of the Pisia and Skinos Faults using corrugated sheets to explain the change in slip direction along the faults. (d) Possible rupture sequence based on mean slip vectors and a geometric barrier. (For interpretation of the references to colour in this figure legend, the reader is referred to the Web version of this article.)

perhaps the bends have a role to play in perturbing the stress on the fault across strike.

However, the role of bends is complicated. It has been shown that bends in fault strike, often associated with changes in dip, can increase the surface slip expected within the bend (Faure Walker et al., 2009; Mildon et al., 2016; Iezzi et al., 2018, 2020). In this paper, we have documented examples where bends are associated with anomalously high surface slip, but we have also found examples where this does not occur. For example, between 675,000 and 677,000 on the Skinos Fault a peak in slip coincides with a change in the overall strike of 30–40° in the map trace (compare Fig. 4avii and 4av) and the perhaps an increase in dip (Fig. 4aii). Another example exists on the Pisia Fault between 677, 000 and 679,000 where a peak in slip coincides with a change in the overall strike of 40–45° in the map trace (compare Fig. 4bvii and 4bv), again with an increase in fault dip. In contrast, the major bend in the fault trace of the Skinos Fault between 679,000 and 681,000 is not associated with a peak in surface slip, despite high values of dip, but there is a nearby peak in slip on the Pisia Fault across strike which may influence the Skinos Fault with its low surface slip at that location. So, bends do not always produce an increase in surface slip and it is unclear whether bends influence slip across strike, however, this may well be a geometrical difference between the Pisia-Skinos example and those shown in Fig. 1.

Another complexity is that the zone of overlap between the Pisia and Skinos Faults is only ~8–10 km sub-parallel to the fault strikes, with the Pisia Fault extending further west for ~10 km and the Skinos Fault extending east for ~20 km (Fig. 2); the interaction evidenced by the coseismic slip profiles does not cover the entire lengths of the faults. Moreover, within the overlap zone, the slip vectors are approximately north-south on the Pisia Fault, but north-east – south-west on the Skinos Fault (Fig. 5) (Roberts, 1996). Thus, due to complex kinematics with slip on the two faults not sharing the same slip-vector azimuth, it is challenging to see how the north coseismic motions of the Pisia ruptures could occur on the Skinos Fault, given its geometry, which favours slip to the north-west. This is reminiscent of kinematic barriers described by Aki (1979). For example, Fig. 5 shows that the b-axis calculations reveal the corrugated nature of the faults, and corrugations plunge north on the Pisia Fault and north-east on the Skinos Fault, so it is hard to envisage how slip to the north could occur on the Skinos Fault. This is shown in more detail on Fig. 8, where we simplify the situation to aid explanation and draw simplified corrugated surfaces. Perhaps it is the mismatch in slip vector and corrugation orientations that caused the ruptures to split onto the Pisia and Skinos Faults, perhaps even in separate earthquakes, although this is uncertain. It may also be that the major bend in the Pisia Fault between ~678,500 and 680,000, with a clear change in b-axis orientation compared to the rest of the Pisia Fault (see Fig. 5b AreaP4), did not allow this portion of the fault to participate in slip to the north, but did allow it to participate in slip to the north-east along with slip on the Skinos Fault. This speculative rupture scenario of parts of each fault ruptured in each event is shown in Fig. 8, but the reader should bear in mind that both earthquakes occurred overnight, and it is unclear which fault or portions of the fault ruptured in each earthquake.

With the unknowns discussed above we are still faced with real-world practical problems, and these are described and discussed in turn below. Detailed analysis of fault geometries and slip kinematics have been highlighted by the ESC working group Fault2SHA as critical in improving earthquake hazard and risk estimates (Faure Walker et al., 2019, 2021). Field investigations of faults such as the one provided herein contributes relevant observations toward improving seismic hazard assessments and so we suggest future studies to be undertaken with a similar analysis on other coseismic ruptures. The displacements across surface ruptures produced by earthquakes pose significant hazard to people, buildings, and infrastructure on or close to the trace of the fault (Bryant and Hart, 1999; Youngs et al., 2003; Testa et al., 2021; Iezzi et al., 2023), and empirical data on surface displacements may be useful as a guide to expected displacements given information on fault length

and position relative to the fault. However, our present study highlights three complications to this approach.

The first complication is that during a normal faulting earthquake sequence, unlike the examples shown in Fig. 1, ruptures do not always propagate onto along-strike faults. Instead, successive ruptures may migrate across-strike, like the 1981 ruptures on the Pisia and Skinos Faults, although the faults may possibly link at depth, then subsequently propagating onto the along-strike Kaparelli Fault (Jackson et al., 1982). The across-strike rupture migration would not be postulated if, following the first earthquake, the future earthquake scenario was examined using typical Coulomb stress models as these would assume stress increases only on along-strike faults. Therefore, we highlight that all neighbouring faults, whether along-strike or across-strike, should be considered during assessment of future earthquake locations.

The second complication is that rupture throws do not appear as single smooth symmetrical profiles when measured in the field. The double maxima displacement profile we observed on the Skinos Fault (Fig. 7b) would not have been anticipated if the expected typical bell-shaped or skewed throw profiles were assumed (Walsh and Watterson, 1988; Cowie and Shipton, 1998). The double maxima profile we observed may in fact be produced by a combination of the assumed relationship between displacement and fault distance as mentioned above and across strike displacement deficits on the ruptures of the Pisia and Skinos Faults, in other words the slip is partitioned between the two faults. In addition, the two peaks on the Skinos Fault were observed near the extremities of the zone of fault overlap, and this would also not have been anticipated if a simple relationship between displacement and distance along the fault relative to fault tips and the fault centre were used. Alternatively, the displacement lows may also reflect local off-fault deformation e.g. distributed shear and/or horizontal axis rotations (Walsh et al., 1996).

The third complication is that rupture patterns may change from one earthquake to the next and represent non-characteristic earthquakes (Schwartz and Coppersmith, 1984; Roberts, 1996). Our observations of double lichen-free stripes suggest that the earthquake prior to 1981 on the Pisia Fault had a very different displacement profile to that in 1981, so the two earthquakes are non-characteristic in slip (Fig. 6b and c). It might be expected that the throw profiles would be similar to a typical bell-shaped or skewed distribution (Walsh and Watterson, 1988; Cowie and Shipton, 1998). However, the patterns of the surface displacements appear to be also be influenced by the rupture history of surrounding faults and structural complexity along the fault itself. The rupture style may therefore change from one earthquake to the next.

In summary, it is clear that a number of unknowns exist in terms of the underlying processes that occurred on the Pisia and Skinos Faults during the 1981 earthquake sequence, and hence those shown in Fig. 1, yet we are faced with real-world problems that arise out of the across-strike rupture patterns that we now know exist. We suggest that more work is required studying the geometry and kinematics of normal faulting earthquakes sequences to develop an overarching understanding of the processes involved.

6. Conclusions

Field-based observations and structural measurement analysis of the coseismic ruptures on the sub-parallel Pisia and Skinos Normal Faults produced during the 1981 eastern Gulf of Corinth earthquake sequence imply the following: (1) The faults exhibit no resolvable post-seismic slip in 41 years since the earthquakes. (2) Slip vector convergence and divergence toward the hangingwall may reveal the presence of major fault bends with the support of fault geometry analysis. In addition, slip vector analysis may indicate a rupture sequence scenario. (3) The Pisia and Skinos Faults may interact during the rupture process of earthquakes spaced only a few hours apart in time to produce the overall slip across the combined structure. (4) The Pisia and Skinos Faults produce non-characteristic earthquakes.

We suggest that the key reasons for the ruptures being produced in the overlap zone on the Pisia and Skinos Faults with the generation of two earthquakes likely lies in a combination of the complexity in geometry of each fault, such as fault bends and orientation of corrugations, and the proximity of the two faults to one another. Fault interaction between the Pisia and Skinos Faults may be implied by their coseismic throws as slip deficits in the set of ruptures from one fault seem to be filled in by slip maxima in the set of ruptures from the other fault. Thus, not all the stored elastic strain that accumulated prior to 1981 was released when the first earthquake occurred.

Overall, detailed structural analysis, more specifically throws and slip vectors, of normal faulting ruptures may be key to understanding the faulting process; kinematic measurements have the potential to describe and explain rupture style, earthquake sequences and improve the understanding of seismic hazard.

CRediT authorship contribution statement

Sam Mitchell: Writing – original draft, Visualization, Resources, Project administration, Methodology, Investigation, Funding acquisition, Formal analysis, Data curation, Conceptualization. **Gerald P. Roberts:** Writing – review & editing, Visualization, Supervision, Resources, Methodology, Investigation, Funding acquisition, Formal analysis, Data curation, Conceptualization. **Joanna P. Faure Walker:** Writing – review & editing, Visualization, Supervision, Resources, Methodology, Investigation, Funding acquisition, Formal analysis, Conceptualization. **Francesco Iezzi:** Writing – review & editing. **Claudia Sgambato:** Writing – review & editing, Investigation. **Jennifer Robertson:** Writing – review & editing, Investigation. **Zoë K. Mildon:** Writing – review & editing, Funding acquisition. **Athanassios Ganas:** Writing – review & editing, Resources. **Ioannis D. Papanikolaou:** Writing – review & editing. **Elias J. Rugen:** Writing – review & editing, Investigation.

Declaration of competing interest

The authors declare that they have no known competing financial interests or personal relationships that could have appeared to influence the work reported in this paper.

Data availability

The data in this study is available in the appendices.

Acknowledgements

Appendix A. Supplementary data

Supplementary data to this article can be found online at https://doi.org/10.1016/j.jsg.2024.105117.

References

Abercrombie, R.E., Main, I.G., Douglas, A., Burton, P.W., 1995. The nucleation and rupture process of the 1981 Gulf of Corinth earthquakes from deconvolved broad-band data. Geophys. J. Int. 120, 393–405.

Aki, K., 1979. Characterization of barriers on an earthquake fault. J. Geophys. Res. Solid Earth 84, 6140–6148.

Allmendinger, R.W., Cardozo, N., Fisher, D.M., 2011. Structural Geology Algorithms: Vectors and Tensors. Cambridge University Press.

Ambraseys, N.N., Jackson, J.A., 1990. Seismicity and associated strain of central Greece between 1890 and 1988. Geophys. J. Int. 101, 663–708.

Bello, S., de Nardis, R., Scarpa, R., Brozzetti, F., Cirillo, D., Ferrarini, F., Di Lieto, B., Arrowsmith, R.J., Lavecchia, G., 2021a. Fault pattern and seismotectonic style of the Campania–Lucania 1980 earthquake (Mw 6.9, Southern Italy): new multidisciplinary constraints. Front. Earth Sci. 8, 608063.

Bello, S., Scott, C.P., Ferrarini, F., Brozzetti, F., Scott, T., Cirillo, D., de Nardis, R., Arrowsmith, J.R., Lavecchia, G., 2021b. High-resolution surface faulting from the 1983 Idaho Lost River Fault Mw 6.9 earthquake and previous events. Sci. Data 8, 68.

Bello, S., Andrenacci, C., Cirillo, D., Scott, C.P., Brozzetti, F., Arrowsmith, J.R., Lavecchia, G., Ao, S., 2022. High-detail fault segmentation: deep insight into the anatomy of the 1983 Borah Peak earthquake rupture zone (Mw 6.9, Idaho, USA). Lithosphere 2022.

Biasi, G.P., Wesnousky, S.G., 2017. Bends and ends of surface ruptures. Bull. Seismol. Soc. Am. 107, 2543–2560.

Billiris, H., Paradissis, D., Veis, G., England, P., Featherstone, W., Parsons, B., Cross, P., Rands, P., Rayson, M., Sellers, P., Ashkenazi, V., Davison, M., Jackson, J., Ambraseys, N., 1991. Geodetic determination of tectonic deformation in central Greece from 1900 to 1988. Nature 350, 124–129.

Briole, P., Ganas, A., Elias, P., Dimitrov, D., 2021. The GPS velocity field of the Aegean. New observations, contribution of the earthquakes, crustal blocks model. Geophys. J. Int. 226, 468–492.

Brozzetti, F., Boncio, P., Cirillo, D., Ferrarini, F., De Nardis, R., Testa, A., Liberi, F., Lavecchia, G., 2019. High-resolution field mapping and analysis of the August–October 2016 coseismic surface faulting (central Italy earthquakes): slip distribution, parameterization, and comparison with global earthquakes. Tectonics 38, 417–439.

Bryant, W.A., Hart, E.W., 1999. Fault-rupture Hazard Zones in California: Alquist-Priolo Earthquake Fault Zoning Act with Index to Earthquake Fault Zones Maps, vol. 42. California Department of Conservation, Division of Mines and Geology.

Caskey, S., Wesnousky, S.G., Zhang, P., Slemmons, D.B., 1996. Surface faulting of the 1954 Fairview peak (MS 7.2) and Dixie Valley (MS 6.8) earthquakes, central Nevada. Bull. Seismol. Soc. Am. 86, 761–787.

Clarke, P.J., Davies, R.R., England, P.C., Parsons, B., Billiris, H., Paradissis, D., Veis, G., Cross, P.A., Denys, P.H., Ashkenazi, V., 1998. Crustal strain in central Greece from repeated GPS measurements in the interval 1989-1997. Geophys. J. Int. 135, 195–214.

Collier, R.E.L., Pantosti, D., D'Addezio, G., De Martini, P.M., Masana, E., Sakellariou, D., 1998. Paleoseismicity of the 1981 Corinth earthquake fault: seismic contribution to extensional strain in central Greece and implications for seismic hazard. J. Geophys. Res. Solid Earth 103, 30001–30019.

Cowie, P.A., Shipton, Z.K., 1998. Fault tip displacement profiles and process zone dimensions. J. Struct. Geol. 20, 983–997.

Cowie, P.A., Underhill, J.R., Behn, M.D., Lin, J., Gill, C.E., 2005. Spatio-temporal evolution of strain accumulation derived from multi-scale observations of Late Jurassic rifting in the northern North Sea: a critical test of models for lithospheric extension. Earth Planet Sci. Lett. 234, 401–419.

Crone, A.J., Machette, M.N., Bonilla, M.G., Lienkaemper, J.J., Pierce, K.L., Scott, W.E., Bucknam, R.C., 1987. Surface faulting accompanying the Borah Peak earthquake and segmentation of the lost river fault, central Idaho. Bull. Seismol. Soc. Am. 77, 739–770.

Faure Walker, J.P., Boncio, P., Pace, B., Roberts, G., Benedetti, L., Scotti, O., Visini, F., Peruzza, L., 2021. Fault2SHA Central Apennines database and structuring active fault data for seismic hazard assessment. Scientific Data 8, 87.

Faure Walker, J.P., Roberts, G.P., Cowie, P.A., Papanikolaou, I.D., Sammonds, P.R., Michetti, A.M., Phillips, R.J., 2009. Horizontal strain-rates and throw-rates for breached relay-zones: an example from active normal faults in the Apennines, Italy. J. Struct. Geol. 31, 1145–1160.

Faure Walker, J.P., Roberts, G.P., Sammonds, P.R., Cowie, P.A., 2010. Comparison of earthquake strains over 10^2 and 10^4 year timescales: insights into variability in the seismic cycle in the central Apennines, Italy. J. Geophys. Res. 115, B10418.

Faure Walker, J.P., Visini, F., Roberts, G.P., Galasso, C., McCaffrey, K., Mildon, Z., 2019. Variable fault geometry suggests detailed fault-slip-rate profiles and geometries are needed for fault-based probabilistic seismic hazard assessment (PSHA). Bull. Seismol. Soc. Am. 109, 110–123.

Ford, M., Rohais, S., Williams, E.A., Bourlange, S., Jousselin, D., Backert, N., Malartre, F., 2013. Tectono-sedimentary evolution of the western Corinth rift (Central Greece). Basin Res. 25, 3–25.

Ganas, A., Oikonomou, A., Tsimi, C., 2013. Noafaults: a digital database for active faults in Greece. National Documentation Centre 47, 518–530.

Ganas, A., Roberts, G.P., Memou, T., 1998. Segment boundaries, the 1894 ruptures and strain patterns along the Atalanti fault, central Greece. J. Geodyn. 26, 461–486.

Gawthorpe, R.L., Fabregas, N., Pechlivanidou, S., Ford, M., Collier, R.E.L., Carter, G.D., McNeill, L.C., Shillington, D.J., 2022. Late Quaternary mud-dominated, basin-floor sedimentation of the Gulf of Corinth, Greece: implications for deep-water depositional processes and controls on syn-rift sedimentation. Basin Res. 34, 1567–1600.

Gawthorpe, R.L., Leeder, M.R., Kranis, H., Skourtsos, E., Andrews, J.E., Henstra, G.A., Mack, G.H., Muravchik, M., Turner, J.A., Stamatakis, M., 2018. Tectono-sedimentary evolution of the plio-pleistocene Corinth rift, Greece. Basin Res. 30, 448–479.

Goldsworthy, M., Jackson, J., 2000. Active normal fault evolution in Greece revealed by geomorphology and drainage patterns. J. Geol. Soc. 157, 967–981.

Goldsworthy, M., Jackson, J., Haines, J., 2002. The continuity of active fault systems in Greece. Geophys. J. Int. 148, 596–618.

Guidoboni, E., Traina, G., Comastri, A., 1994. Catalogue of Ancient Earthquakes in the Mediterranean Sea up to the 10th Century.

Gupta, S., Cowie, P.A., Dawers, N.H., Underhill, J.R., 1998. A mechanism to explain rift-basin subsidence and stratigraphic patterns through fault-array evolution. Geology 26, 595–598.

Gupta, A., Scholz, C.H., 2000. A model of normal fault interaction based on observations and theory. J. Struct. Geol. 22, 865–879.

Hubert, A., King, G., Armijo, R., Meyer, B., Papanastasiou, D., 1996. Fault re-activation, stress interaction and rupture propagation of the 1981 Corinth earthquake sequence. Earth Planet Sci. Lett. 142, 573–585.

Iezzi, F., Boncio, P., Testa, A., Giulio, G.D., Vassallo, M., Cara, F., Milana, G., Galadini, F., Giaccio, B., Luca, M.D., 2023. A case study of multidisciplinary surface faulting assessment in the urbanized fucino basin, Italy. Italian Journal of Geosciences 142, 104–121.

Iezzi, F., Mildon, Z., Faure Walker, J.P., Roberts, G., Goodall, H., Wilkinson, M., Robertson, J., 2018. Coseismic throw variation across along-strike bends on active normal faults: implications for displacement versus length scaling of earthquake ruptures. J. Geophys. Res. Solid Earth 123, 9817–9841.

Iezzi, F., Roberts, G., Faure Walker, J.P., Papanikolaou, I., 2019. Occurrence of partial and total coseismic ruptures of segmented normal fault systems: insights from the Central Apennines, Italy. J. Struct. Geol. 126, 83–99.

Iezzi, F., Roberts, G., Faure Walker, J.P., Papanikolaou, I.D., Ganas, A., Deligiannakis, G., Beck, J., Wolfers, S., Gheorghiu, D., 2021. Temporal and spatial earthquake clustering revealed through comparison of millennial strain-rates from 36Cl cosmogenic exposure dating and decadal GPS strain-rate. Sci. Rep. 11, 23320.

Iezzi, F., Roberts, G., Faure Walker, J.P., 2020. Throw-rate variations within linkage zones during the growth of normal faults: case studies from the Western Volcanic Zone, Iceland. J. Struct. Geol. 133, 103976.

Jackson, J., 1994. Active tectonics of the Aegean region. Annu. Rev. Earth Planet Sci. 22, 239–271.

Jackson, J., Gagnepain, J., Houseman, G.A., King, G.C., Papadimitriou, P., Soufleris, C., Virieux, J.V., 1982. Seismicity, normal faulting, and the geomorphological development of the gulf of Corinth (Greece): the Corinth earthquakes of february and March 1981. Earth Planet Sci. Lett. 57, 377–397.

Jolivet, L., 2001. A comparison of geodetic and finite strain pattern in the Aegean, geodynamic implications. Earth Planet Sci. Lett. 187, 95–104.

Jolivet, L., Daniel, J.M., Truffert, C., Goffé, B., 1994. Exhumation of deep crustal metamorphic rocks and crustal extension in arc and back-arc regions. Lithos 33, 3–30.

Jolivet, L., Faccenna, C., Huet, B., Labrousse, L., Le Pourhiet, L., Lacombe, O., Lecomte, E., Burov, E., Denèle, Y., Brun, J.-P., Philippon, M., Paul, A., Salaün, G., Karabulut, H., Piromallo, C., Monié, P., Gueydan, F., Okay, A.I., Oberhänsli, R., Pourteau, A., Augier, R., Gadenne, L., Driussi, O., 2013. Aegean tectonics: strain localisation, slab tearing and trench retreat. Tectonophysics 597–598, 1–33.

Kelletat, D., Kowalczyk, G., Schröder, B., Winter, K.-P., 1976. A synoptic view on the neotectonic development of the peloponnesian coastal regions. Z. Dtsch. Geol. Ges. 127, 447–465.

King, G.C.P., Stein, R.S., Lin, J., 1994. Static stress changes and the triggering of earth-quakes. Bull. Seismol. Soc. Am. 84, 935–953.

Le Pichon, X., Angelier, J., 1979. The Hellenic arc and trench system: a key to the neotectonic evolution of the eastern Mediterranean area. Tectonophysics 60, 1–42.

Le Pichon, X., Chamot-Rooke, N., Lallemant, S., Noomen, R., Veis, G., 1995. Geodetic determination of the kinematics of central Greece with respect to Europe: implications for eastern Mediterranean tectonics. J. Geophys. Res. Solid Earth 100, 12675–12690.

McLeod, A.E., Dawers, N.H., Underhill, J.R., 2000. The propagation and linkage of normal faults: insights from the Strathspey–Brent–Statfjord fault array, northern North Sea. Basin Res. 12, 263–284.

Mechernich, S., Schneiderwind, S., Mason, J., Papanikolaou, I.D., Deligiannakis, G., Pallikarakis, A., Binnie, S.A., Dunai, T.J., Reicherter, K., 2018. The seismic history of the Pisia fault (eastern Corinth rift, Greece) from fault plane weathering features and cosmogenic 36Cl dating. J. Geophys. Res. Solid Earth 123, 4266–4284.

Meyer, V., Nicol, A., Childs, C., Walsh, J.J., Watterson, J., 2002. Progressive localisation of strain during the evolution of a normal fault population. J. Struct. Geol. 24, 1215–1231.

Mildon, Z.K, Roberts, G.P., Faure Walker, J.P., Wedmore, L.N., McCaffrey, K.J., 2016. Active normal faulting during the 1997 seismic sequence in Colfiorito, Umbria: did slip propagate to the surface? J. Struct. Geol. 91, 102–113.

Mildon, Z.K., Roberts, G.P., Faure Walker, J.P., Iezzi, F., 2017. Coulomb stress transfer and fault interaction over millennia on non-planar active normal faults: the Mw 6.5–5.0 seismic sequence of 2016–2017, central Italy. Geophys. J. Int. 210, 1206–1218.

Pantosti, D., De Martini, P.M., Papanastassiou, D., Palyvos, N., Lemeille, F., Stavrakakis, G., 2001. A reappraisal of the 1894 Atalanti earthquake surface ruptures, central Greece. Bull. Seismol. Soc. Am. 91, 760–780.

Pantosti, D., Valensise, G., 1990. Faulting mechanism and complexity of the November 23, 1980, Campania-Lucania Earthquake, inferred from surface observations. J. Geophys. Res. Solid Earth 95, 15319–15341.

Roberts, G.P., 1996. Noncharacteristic normal faulting surface ruptures from the Gulf of Corinth, Greece. J. Geophys. Res. Solid Earth 101, 25255–25267.

Roberts, G.P., Ganas, A., 2000. Fault-slip directions in central and southern Greece measured from striated and corrugated fault planes: comparison with focal mechanism and geodetic data. J. Geophys. Res. Solid Earth 105, 23443–23462.

Roberts, G.P., 1996. Variation in fault-slip directions along active and segmented normal fault systems. J. Struct. Geol. 18, 835–845.

Roberts, G.P., 2007. Fault orientation variations along the strike of active normal fault systems in Italy and Greece: implications for predicting the orientations of subseismic-resolution faults in hydrocarbon reservoirs. AAPG Bull. 91, 1–20.

Roberts, G., Houghton, S.L., Underwood, C., Papanikolaou, I., Cowie, P.A., van Calsteren, P., Wigley, T., Cooper, F.J., McArthur, J.M., 2009. Localization of Quaternary slip rates in an active rift in 105 years: An example from central Greece constrained by 234U-230Th coral dates from uplifted paleoshorelines. J. Geophys. Res. Solid Earth 114.

Roberts, S., Jackson, J., 1991. Active Normal Faulting in Central Greece: an Overview, vol. 56. Geological Society, London, Special Publications, pp. 125–142.

Rohais, S., Eschard, R., Ford, M., Guillocheau, F., Moretti, I., 2007. Stratigraphic architecture of the plio-pleistocene infill of the Corinth rift: implications for its structural evolution. Tectonophysics 440, 5–28.

Schwartz, D.P., Coppersmith, K.J., 1984. Fault behavior and characteristic earthquakes: examples from the Wasatch and San Andreas fault zones. J. Geophys. Res. Solid Earth 89, 5681–5698.

Stein, R.S., 1999. The role of stress transfer in earthquake occurrence. Nature 402, 605–609.

Suter, M., 2015. Rupture of the Pitáycachi fault in the 1887 Mw 7.5 Sonora, Mexico earthquake (southern Basin-and-Range Province): rupture kinematics and epicenter inferred from rupture branching patterns. J. Geophys. Res. Solid Earth 120, 617–641.

Taylor, B., Weiss, J.R., Goodliffe, A.M., Sachpazi, M., Laigle, M., Hirn, A., 2011. The structures, stratigraphy and evolution of the Gulf of Corinth rift, Greece. Geophys. J. Int. 185, 1189–1219.

Testa, A., Valentini, A., Boncio, P., Pace, B., Visini, F., Mirabella, F., Pauselli, C., 2021. Probabilistic fault displacement hazard analysis of the Anghiari-Città di Castello normal fault (Italy). Italian Journal of Geosciences 140, 327–346.

Vassilakis, E., Royden, L., Papanikolaou, D., 2011. Kinematic links between subduction along the Hellenic trench and extension in the Gulf of Corinth, Greece: a multidisciplinary analysis. Earth Planet Sci. Lett. 303, 108–120.

Villani, F., Pucci, S., Civico, R., De Martini, P.M., Cinti, F.R., Pantosti, D., 2018. Surface faulting of the 30 october 2016 Mw 6.5 Central Italy earthquake: detailed analysis of a complex coseismic rupture. Tectonics 37, 3378–3410.

Walker, R.T., Claisse, S., Telfer, M., Nissen, E., England, P., Bryant, C., Bailey, R., 2010. Preliminary estimate of Holocene slip rate on active normal faults bounding the southern coast of the Gulf of Evia, central Greece. Geosphere 6, 583–593.

Walsh, J.J., Watterson, J., 1988. Analysis of the relationship between displacements and dimensions of faults. J. Struct. Geol. 10, 239–247.

Walsh, J.J., Watterson, J., Childs, C., Nicol, A., 1996. Ductile Strain Effects in the Analysis of Seismic Interpretations of Normal Fault Systems, vol. 99. Geological Society, London, Special Publications, pp. 27–40.

Westaway, R., 1991. Continental Extension on Sets of Parallel Faults: Observational Evidence and Theoretical Models, vol. 56. Geological Society, London, Special Publications, pp. 143–169.

Whittaker, A.C., Walker, A.S., 2015. Geomorphic constraints on fault throw rates and linkage times: examples from the Northern Gulf of Evia, Greece. J. Geophys. Res.: Earth Surf. 120, 137–158.

Youngs, R.R., Arabasz, W.J., Anderson, R.E., Ramelli, A.R., Ake, J.P., Slemmons, D.B., McCalpin, J.P., Doser, D.I., Fridrich, C.J., Swan III, F.H., 2003. A methodology for probabilistic fault displacement hazard analysis (PFDHA). Earthq. Spectra 19, 191–219.